Journal of Fluorescence
https://doi.org/10.1007/s10895-023-03495-7

RESEARCH

Construction and Application of Fluorescent Probes with Imine Protective Groups for Hypochlorite Detection

Junyang Zhu[1] · Zhaoye Lyu[1] · Yulan Qian[1] · Hailong Cui[1] · Yutao Feng[1] · Miao Li[2] · Lihua Lyu[1] · Hongjuan Zhao[1] · Chengqi Jiao[3] · Xiaoqing Xiong[1]

Received: 9 October 2023 / Accepted: 6 November 2023

Abstract

Several fluorescent probes have been designed to detect ClO^- in biological systems based on the isomerization mechanism of C=N bonds. Particularly, fluorescein has emerged as an important fluorophore for detecting ClO^- because of its unique properties. Previously, we introduced the fluorescein analog **F-1** with an active aldehyde group. In this study, two ClO^- fluorescent sensors (**F-2** and **F-3**) with imine groups were designed and synthesized using diaminomaleonitrile and 2-hydrazylbenzothiazole as amines. The electron cloud distribution of **F-2** and **F-3** in ground and excited states was explored via Gaussian calculations, reasonably explaining their photophysical properties. The fluorescence detection of ClO^- in solution using the two probes (**F-2** and **F-3**) was realized based on the mechanism of imine deprotection with ClO^-. NaClO concentration titration demonstrated that the colorimetric detection of ClO^- with the naked eye could be achieved using both **F-2** and **F-3**. However, after adding ClO^-, the fluorescence intensity of probe **F-2** increased, whereas that of probe **F-3** first decreased and then increased. Probes **F-2** and **F-3** exhibited good selectivity, anti-interference capability, and sensitivity, with the detection limits of 169.95 and 37.30 μM, respectively. Owing to their low cell toxicity, probes **F-2** and **F-3** can be applied to detect ClO^- in vivo. The design approach adopted in this study will further advance the future development of ClO^- chemical probes through the removal of C=N bond isomerization.

Keywords Hypochlorite probe · Imine protective group · Fluorescent probe · Fluorescence imaging

Introduction

Reactive oxygen species (ROS) are constantly generated during cellular metabolism. ClO^-, which is an oxidized product of the reaction between chloride ions (Cl^-) and H_2O_2 that occurs in the presence of the enzyme myeloperoxidase, is an important ROS and plays a vital role in maintaining the normal functioning of the immune system [1–4]. Owing to the strong oxidizing and antibacterial activity of ClO^-, it has been widely used in household bleach, drinking water disinfection, sewage purification, cooling-water treatment, and paper and textile industries for bleaching [3, 5]. The excessive production and insufficient excretion of ClO^- have been demonstrated to result in several diseases, such as neurodegenerative disorders, atherosclerosis, and cancer [6–10]. Furthermore, the abnormal content of ClO^- can be detrimental to living organisms and environment. Therefore, the development of highly sensitive and selective probes is essential for monitoring the ClO^- level in biological and environmental systems. Fluorescence analysis has emerged as an effective tool for detecting target analysts, and it has unique advantages in terms of sensitivity, selectivity, temporal and spatial resolution, real-time monitoring, biocompatibility, and operational simplicity [11–13].

Junyang Zhu and Zhaoye Lyu contributed equally to this work.

✉ Chengqi Jiao
jiaocq@lnnu.edu.cn

✉ Xiaoqing Xiong
xxq890108@163.com

[1] School of Textile and Material Engineering, Dalian Polytechnic University, #1 Qinggongyuan, Dalian 116034, China

[2] School of Biological Engineering, Dalian Polytechnic University, #1 Qinggongyuan, Dalian 116034, China

[3] School of Chemistry and Chemical Engineering, Liaoning Normal University, 850 Huanghe Road, Dalian 116029, China

Published online: 17 November 2023

Recently, several probes that can detect ClO^- have been designed and synthesized based on various mechanisms, including the oxidation of hydrazide [14], phenothiazine [15], phenol [16], oxime [17–19], double bond [20], and diphenylphosphine [21]. Among these mechanisms, the oxidation of the C = N bond in fluorophores, which was synthesized via the protection of aldehyde groups as oximes, is an important aspect for ClO^- detection. These probes can be fluorescent-free or fluorescent based on the isomerization mechanism. An effective strategy for recovering/quenching fluorescence is to remove the C = N bond in the sensor by promoting the specific deprotection reactions of oximes with special analytes [22–24]. A series of highly selective probes based on different fluorophores has been developed to detect the analyte ClO^- [19, 25, 26]. Particularly, fluorescein has emerged as an important fluorophore for ClO^- detection. The fluorescein structure has been continuously modified, and several fluorescent probes have been designed and synthesized for detecting ClO^- owing to the advantages of fluorescein, such as good water solubility, excitation and emission wavelengths in the visible-light region, and high fluorescence quantum yield [23, 27, 28]. Therefore, the development of fluorescent sensors based on fluorescein or its derivatives is necessary for the high-performance detection of ClO^-. Previously, we investigated a fluorescein derivative **F-1** containing an aldehyde group (Fig. 1) [29, 30]. The active aldehyde group can react with different amine substances to form imine derivatives, which is beneficial for constructing ClO^- fluorescent probes. Dye **F-1** possesses excellent photophysical properties, exhibiting a high fluorescence quantum yield (Φ) in polar protic solvents and large Stokes shift (123 nm) in various solvents [30]. Therefore, **F-1** derivatives can be constructed by regulating the amines reacting with aldehyde to introduce imine groups into **F-1**.

Based on the aforementioned considerations, two new ClO^- fluorescent sensors (**F-2** and **F-3**) with an imine group were designed and synthesized via the reaction of two different amines with the fluorescein derivative **F-1** (Fig. 1). The compounds **F-2** and **F-3** comprised the fluorescein derivative and an imine protection group as the recognition unit. The imine group can be deprotected by ClO^- to release an aldehyde group, which is accompanied by changes in the "OFF–ON" or "ON–OFF" signal. The fluorescence and absorption responses of **F-2** and **F-3** correlate with the ClO^- concentration and are due to the oxidization of the sensor by ClO^-. Furthermore, Gaussian calculations were used to explain the photophysical properties and clarify the absorbance and emission spectra of **F-2** and **F-3**. Additionally, the cell permeability and cytotoxicity of **F-2** and **F-3** were analyzed to demonstrate their potential for application in biology. The design approach adopted in this study will broaden the platform for the future development of ClO^- chemical sensors through the removal of C = N bonds.

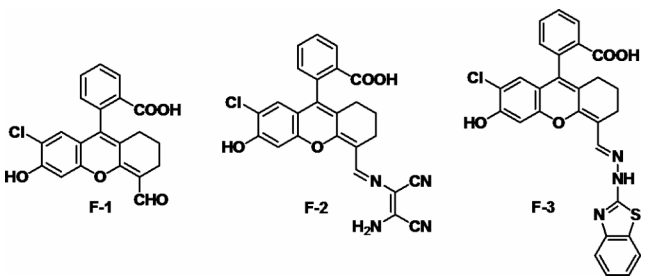

Fig. 1 The structures of **F-1**, **F-2**, and **F-3**

Experimental Section

Synthesis of F-1

The detailed synthesis routines for **F-1** can be found in the literature (Scheme S1) [28].

Synthesis of Probe F-2

F-1 (0.13 g, 0.335 mmol) and diaminomaleonitrile (0.19 g, 1.770 mmol) were dissolved in CH_3CH_2OH (15 mL) and then placed into a round-bottomed flask. The reaction mixture was stirred at 85 °C and refluxed for 3.5 h. After completing the reaction, the solution was cooled to room temperature and then dried by a rotary evaporator. Then, after vacuum drying, the purplish red was separated and purified by column chromatography (CH_2Cl_2/CH_3OH = 200/3). The yield was obtained as 71% on the basis of chromatography The target product fluorescent probe **F-2** (0.113 g, 0.239 mmol) was obtained. ^{1} H NMR (400 MHz, DMSO-d_6) ^{1} H NMR (400 MHz, DMSO-d_6) δ 8.63 (s, 1 H), 8.06 (d, J = 7.7 Hz, 1 H), 7.70 (t, J = 7.5 Hz, 1 H), 7.58 (t, J = 7.9 Hz, 1 H), 7.22 (d, J = 7.4 Hz, 1 H), 7.16 (d, J = 14.4 Hz, 2 H), 6.77 (s, 1 H), 6.30 (s, 1 H), 2.11 (dt, J = 17.3, 6.7 Hz, 2 H), 1.58 (dt, J = 12.0, 6.3 Hz, 2 H), 0.86 (t, J = 6.7 Hz, 2 H). ^{13} C NMR (100 MHz, DMSO-d_6) δ 155.01, 154.81, 151.38, 151.29, 135.63, 135.60, 132.49, 130.95, 130.37, 128.92, 125.79, 123.76, 123.24, 116.40, 115.50, 115.26, 114.40, 112.11, 106.69, 103.16, 29.57, 27.55, 23.32, 22.76, 20.51, 14.45. Found: C, 63.55%; H, 3.52%; N, 11.80%; O, 13.58%; molecular formula $C_{25}H_{17}ClN_4O_4$ requires C, 63.50%; H, 3.62%; N, 11.85%; O, 13.53%. HRMS Found: $[M+H]^-$ 471.0871; molecular formula $C_{25}H_{17}ClN_4O_4$ requires $[M+H]^-$ 472.0938.

Synthesis of Probe F-3

F-1 (0.10 g, 0.268 mmol) and 2-hydrazylbenzothiazole (0.09 g, 0.555 mmol) were dissolved in CH_3CH_2OH (15 mL) and then placed into a round-bottomed flask. **F-3** was synthesized and purified by the analogous method as that used to obtain **F-2**. Then, after vacuum drying, the yellow solid preliminary product was obtained by column chromatography ($CH_2Cl_2/CH_3OH = 200/5$). After preliminary purification, add a small amount of Na_2CO_3 to the solution of preliminary product in CH_3CH_2OH and then reflux for 6 h. The purified product fluorescent probe **F-3** (0.074 g, 0.140 mmol) was obtained. ^{1}H NMR (400 MHz, DMSO-d_6) δ 8.46 (s, 1 H), 8.02 (d, J = 7.8 Hz, 1 H), 7.72 (s, 2 H), 7.59 (t, J = 7.7 Hz, 1 H), 7.43 (d, J = 7.9 Hz, 1 H), 7.27 (t, J = 8.2 Hz, 2 H), 7.07 (t, J = 7.5 Hz, 1 H), 6.66 (s, 1 H), 6.20 (s, 1 H), 2.10 (d, J = 12.9 Hz, 2 H), 2.06–1.94 (m, 2 H), 1.57 (h, J = 6.5 Hz, 2 H). ^{13}C NMR (100 MHz, DMSO) δ 167.83, 167.15, 154.13, 151.45, 149.83, 133.03, 130.95, 130.11, 129.06, 126.26, 125.38, 123.57, 121.83, 121.69, 116.69, 114.24, 109.53, 103.16, 68.97, 63.26, 56.30, 35.58, 32.56, 31.74, 30.07, 29.49, 29.28, 29.15, 29.04, 27.52, 27.02, 25.56, 25.26, 23.17, 22.55, 20.50, 14.41. Found: C, 63.35%; H, 3.85%; N, 7.98%; O, 12.13%; S, 6.10%; molecular formula $C_{28}H_{20}ClN_3O_4S$ requires C, 63.45%; H, 3.80%; N, 7.93; O, 12.08%; S, 6.05%. HRMS Found: $[M - H]^-$ 528.0793; molecular formula $C_{28}H_{20}ClN_3O_4S$ requires $[M - H]^-$ 528.0785.

Results and Discussion

Synthesis and Photophysical Properties of Fluorescent Probes F-2 and F-3

Generally, the fluorophores containing C = N bonds are non-fluorescent or weakly fluorescent. Therefore, fluorescent probes **F-2** and **F-3** were prepared via the reaction of the fluorescein derivative **F-1** with 2-hydrazylbenzothiazole and diaminomaleonitrile (Schemes S1 and S2). During preparation, the yields of probes **F-2** and **F-3** were monitored via liquid chromatography–mass spectrometry (LC–MS). Notably, the mass spectrum of **F-3** always indicated the presence of a certain by-product with a molecular weight of 530.1 g/mol (Fig. S1), and the unknown product accounted for 85.619% of the total product (Table S1). Comparing the precise molecular weight of probe **F-3** (529.08 g/mol) with the molecular weight of the unknown product, the latter has approximately one proton less than probe **F-3**. Considering that the carboxyl group on the benzene ring of the fluorescein-like fluorophore easily closes to form a *penta*-membered spirocyclic ester, the by-product is presumed to be the ring-closed structure **F-3'** of probe **F-3** (Scheme S3). To completely convert byproduct **F-3'** into probe **F-3**, a small amount of Na_2CO_3 was added to the solution of preliminary product **F-3**. Unexpectedly, by-product **F-3'** can be converted into target probe **F-3** with a high yield (100%) by refluxing it for 6 h.

After purifying the preliminary products **F-2** and **F-3**, their absorption and emission spectra were investigated. From Tables S2 and S3, the maximum absorption range in the spectra of probes **F-2** and **F-3** is 471–494 nm and 431–438 nm, respectively. The maximum emission wavelengths of probes **F-2** and **F-3** range from 531 to 574 nm and 527 to 578 nm, respectively. Compared with that of probe **F-3**, the absorption wavelength of probe **F-2** is redshifted, which may be attributed to the presence of two nitrile groups with strong electron withdrawing ability in the structure of probe **F-2**. Comparing with those of conventional fluorescein derivatives, the Stokes shifts of probes **F-2** and **F-3** are larger (48 nm), which is consistent with the predicted result and is beneficial for future applications. Furthermore, the fluorescence quantum yields for **F-2** and **F-3** in different solvents are summarized in Tables S2 and S3. The fluorescence quantum yields of probe **F-2** were lower than those of probe **F-3**, and probe **F-2** exhibited negligible fluorescence. Although probe **F-3** exhibited weak fluorescence in various solvents, the fluorescence quantum yield of **F-3** remained lower than that of **F-1**. In summary, the isomerization of the C = N bond in fluorophores leads to a reduction in the fluorescence quantum yield.

Density Functional Theory (DFT)/Time-Dependent DFT Study of Fluorescent Probes F-2 and F-3

To analyze the photophysical properties and the reason for the low fluorescence quantum yield of probes **F-2** and **F-3**, the absorption and emission spectra of probes **F-2** and **F-3** in dimethyl sulfoxide (DMSO) were determined using the B3LYP/6-311G (d, p) basis set, and the frontier molecular orbitals of the probes were analyzed. The strongest absorption band in the spectrum of probe **F-2** is mainly attributed to the electronic transition from the ground state (S_0) to the excited state (S_1). The resulting transition occurs from the highest occupied molecular orbital (HOMO) to the lowest unoccupied molecular orbital (LUMO), and the oscillator strength (f_{ab}) is estimated as 0.8586 (Fig. 2). The calculated absorption wavelength (λ_{ab}) is 483.54 nm (Table S4). The electron cloud of LUMO is distributed within xanthene and diaminomaleonitrile moieties on the left. The electron cloud of HOMO is also mainly distributed in these two parts; however, the distribution density is slightly different (Fig. 2). Furthermore, considering the emission spectrum of probe **F-2**, the emission wavelength is mainly attributed to

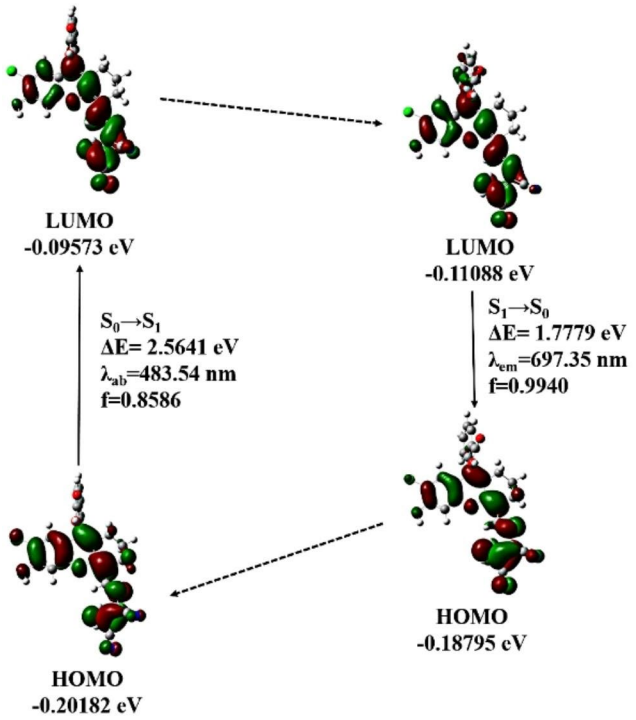

Fig. 2 The frontier molecular orbital diagram for probe **F-2** in DMSO solvent, the left column is the calculation for absorption spectrum which is based on the optimized S_0, and the right column is the calculation of emission spectrum which is based on the optimal S_1

the electronic transition from S_1 to S_0, which occurs from LUMO to HOMO. The calculated emission wavelength λ_{em} and f_{ab} values are 697.35 nm and 0.9940, respectively (Table S5). The LUMO electron cloud is distributed on the left part of oxanthene, diaminomaleonitrile, and benzoic acid, whereas the electron cloud of HOMO is distributed on the left part of oxanthene and diaminomaleonitrile (Fig. 2). A significant charge transfer occurs in the electron cloud from LUMO to HOMO. However, all the wave function excitation coefficients (CI) for the $S_1 \rightarrow S_0$ transition are negative (Table S5). A negative CI value indicates that the $S_1 \rightarrow S_0$ transition is prohibited. Therefore, probe **F-2** exhibited negligible fluorescence in the DMSO solvent, confirming the photophysical property of probe **F-2** in DMSO with a low fluorescence quantum yield.

Furthermore, the electron cloud distribution of probe **F-3** was determined via Gaussian calculations to explore the origin of its fluorescence. Based on DFT, Gaussian calculations were performed for the absorption and emission spectra of probe **F-3** using the B3LYP/6-311G (d, p) basis set, and the frontier molecular orbitals of probe **F-3** were analyzed. The calculation results indicate that the strongest absorption band of probe **F-3** mainly originates from the $S_0 \rightarrow S_1$ transition, which corresponds to the electron leap from HOMO to LUMO (Fig. S2). The corresponding f_{ab} value is 1.3082, and the calculated absorption wavelength λ_{ab} is 452.84 nm (Table S6). Additionally, the emission spectrum of probe **F-3** was determined. The calculated data reveal that the emission wavelength mainly originates from the $S_1 \rightarrow S_0$ transition, corresponding to the electron leap from LUMO to HOMO with an f_{ab} of 1.1284. The calculated emission wavelength λ_{em} is 664.24 nm (Table S7), which is larger than the measured emission wavelength of probe **F-3** in DMSO. However, the calculated Stokes shift (111.40 nm) is similar to the actual Stokes shift (124 nm) in DMSO. Therefore, the calculated result is consistent with the actual measured value, and the error between the calculated and actual values is within the permissible range, which confirms that probe **F-3** exhibits fluorescence and large Stokes shifts in DMSO. Additionally, the LUMO electron cloud is mainly distributed on the benzoic acid, xanthene, and hydrazine moieties, whereas the HOMO orbital electron cloud is primarily distributed on the xanthene and hydrazine benzothiazole parts (Fig. S2). A distinct charge separation phenomenon occurs from LUMO to HOMO, which may have resulted in the large Stokes shift of **F-3**.

Titration of Fluorescent Probes F-2 and F-3 with pH

To investigate the suitability of probes **F-2** and **F-3** during pH variation, fluorescence changes to different pH values were obtained (Figs. S3 and S4), which describes the fluorescent intensity at 545 and 555 nm as a function of pH. As seen from Fig. S3, the fluorescent intensity at 545 nm for **F-2** decreases slowly from 2.24 to 6.15 (Fig. S3A), then a sharp increase appears within a pH range of 6.15 to 13.91 (Fig. S3B). Thus, the pKa for **F-2** was calculated to be 4.00 and 11.56, respectively. The fluorescent intensity at 555 nm for **F-3** also increases slowly from 2.57 to 6.73, a sharp increase appears within a pH range of 6.73 to 10.20, and becomes steady after that (Fig. S4). The fluorescent enhancement was about 3-fold from 6.73 to 10.20 and the pKa for **F-3** was calculated to be 7.45. The titration of fluorescent probes **F-2** and **F-3** to pH indicates the fluorescence intensity of **F-2** and **F-3** can be affected by different pH. Thus, the fluorescent changes at fixed 7.39 and 7.45 were performed, respectively. It was observed that fluorescent intensity is stable for more than 10 min (Fig. S5), indicating the fluorescence signal can be stable at the fixed pH. The following pH for other detection systems was adjusted to a fixed pH using buffer solution.

Titration of Fluorescent Probes F-2 and F-3 with ClO^-

The concentration titration analysis was conducted to investigate the effects of different ClO^- concentrations on probes **F-2** and **F-3**. After adding different concentrations of NaClO, the absorption and emission spectra of probes **F-2** and **F-3**

were measured (Fig. 3 and S6). From Fig. 3, the absorption intensity of probe **F-2** at 485 nm gradually decreases, and the maximum absorption wavelength of probe **F-2** exhibits a blue shift with increasing ClO^- concentration (Fig. 3A). Under natural light, the color of the **F-2** solution gradually changes from deep red to light red (Fig. 3A). Furthermore, as the ClO^- concentration increased, the maximum emission wavelength gradually shifted from 573.5 to 545 nm, and the fluorescence of the **F-2** solution changed from weak yellowish green to blue under ultraviolet light (inset in Fig. 3B). Additionally, to analyze the ability of probe **F-3** to detect ClO^-, the absorption and emission spectra of probe **F-3** were monitored after adding different concentrations of NaClO (Fig. S6). The absorbance at 333 and 430 nm gradually decreased with an increase in the ClO^- concentration, whereas the absorbance at 560 nm gradually increased. Under natural light, the yellow color of the probe **F-3** solution gradually lightened (Fig. S3A). The corresponding fluorescence intensity at 555 nm gradually decreased, and the peak blue shifted to 545 nm. The fluorescence of probe **F-3** changed from weak yellowish green to blue under ultraviolet light (Fig. S3B). However, the maximum emission wavelength of the probe solutions is not consistent with the color of fluorescence after the complete reaction of the probes with NaClO. Theoretically, the fluorescence corresponding to the emission wavelength of approximately 540 nm should be green; however, the actual color of the probe solution was blue.

To determine the reason for the occurrence of the aforementioned phenomenon, other detection methods should be adopted, and the reaction mechanism of probes **F-2** and **F-3** with NaClO should be elucidated. Here, the mass spectra analysis of the products obtained after the reaction of probes **F-2** and **F-3** with ClO^- was conducted. From Figs. S7 and S8, the peaks associated with probes **F-2** and **F-3** (*m/z* 471.09 $[M–H]^-$ and *m/z* 528.03 $[M–H]^-$) have completely disappeared. Considering a large number of fragments in the mass spectra (Figs. S7 and S8), the peaks at *m/z* 385.05 (or 385.00) and *m/z* 430.59 (or 430.63) can be attributed to the molecular ion peaks of dye **F-1** at $[M+3\ H]^{3+}$ and $[M+2\ H]^{2+}+2[Na]^+$. This confirms that dye **F-1** with the aldehyde group can be generated through the reaction of the C = N bond in probes **F-2** and **F-3** with NaClO. Furthermore, distinct peaks were observed at *m/z* 507.02 or *m/z* 566.57 (Figs. S7 and S8). The peak at *m/z* 507.02 corresponds to the $[M+H]^+$ molecular ion peak of the products obtained after the addition of the C = N bond with the chloride anion in probe **F-2** (Fig. S7) [25]. In the case of probe **F-3**, ClO^- can preferentially attack the hydrazine group or react with C = N. Irrespective of the bond that is first attacked by ClO^-, dye **F-1** is always generated during the reaction. When a high concentration of NaClO was added to the solution containing probe **F-3**, an oxidation reaction occurred, resulting in a product whose spectrum comprises a peak at *m/z* 566.57 (Fig. S8). Based on the aforementioned result, a feasible mechanism of detecting ClO^- for probes **F-2** and **F-3** is proposed in Scheme S4. The fluorescent spectra of probes **F-2** and **F-3** at different NaClO concentrations also support the proposed mechanism. Therefore, the products obtained after the reaction of the two probes with NaClO are in the form of mixtures, which may lead to inconsistencies between the emission spectra and fluorescent performance of the solution after the reaction.

Furthermore, the detection limit of probes **F-2** and **F-3** was estimated via a linear response relationship between the fluorescence or absorbance intensity of probes and NaClO concentration. The fluorescence intensity of **F-2** at 545 nm exhibits a good linear relationship with NaClO in the low-concentration range, and a ClO^- detection limit of 169.95 μM is obtained (Fig. S9). Based on the change trend of the absorption spectra at 560 nm of probe **F-3**, the detection limit of probe **F-3** for ClO^- is calculated as 37.30 μM (Fig. S10). The aforementioned results indicate that probes **F-2** and **F-3** can facilitate a highly sensitive detection of ClO^-.

Response Time and Selectivity of Fluorescent Probes F-2 and F-3 Toward ClO^-

Considering the relevance of the response time of fluorescent probes **F-2** and **F-3**, the time-dependent fluorescent intensities at 545 and 555 nm were monitored at a fixed ClO^- concentration. From Fig. 4, the fluorescence intensity

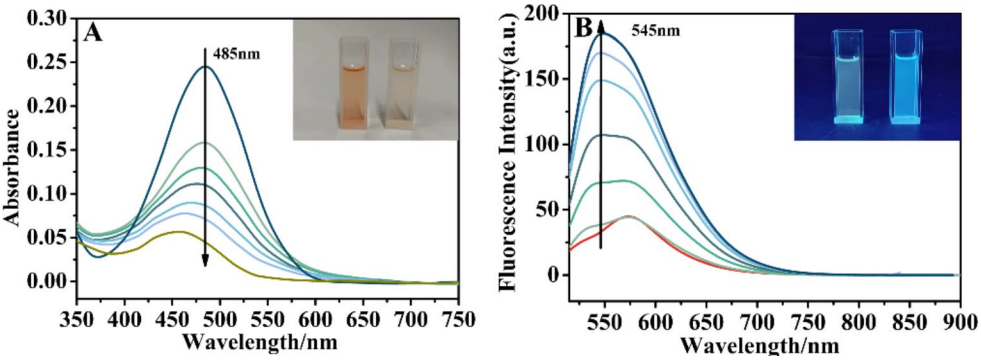

Fig. 3 The spectrum changes of probe **F-2** (15 μM) in CH_3CH_2OH/HEPES buffer after adding different concentrations of NaClO (0→52 eq). **(A)**: the absorption spectra of probe **F-2**, inset shows the color changes of probe **F-2** under natural light; **(B)**: the emission spectra of probe **F-2** with the excitation wavelength at 485 nm, inset shows the color changes of probe **F-2** under ultraviolet light

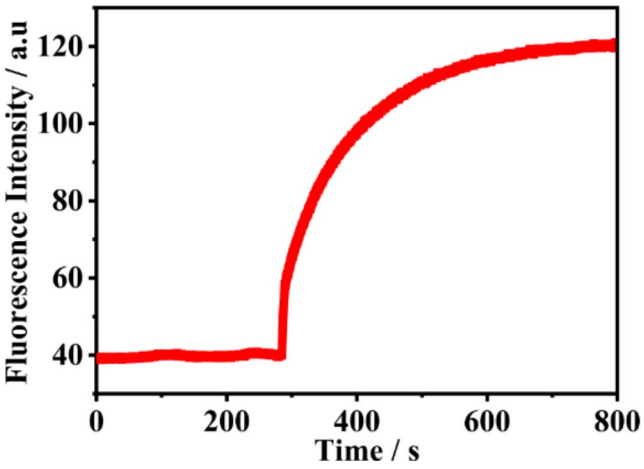

Fig. 4 Time course of the fluorescence response of probe **F-2** (15 μM) in an aqueous solution (CH_3CH_2OH /HEPES buffer = 7/3) with respect to the presence of 52 eq NaClO, the excitation wavelength is 485 nm, and the monitored emission wavelength is 545 nm

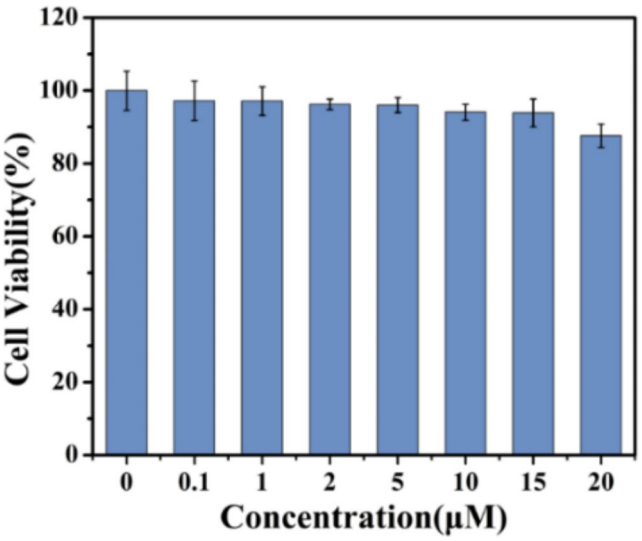

Fig. 5 The cell survival rate of MCF-7 at different concentrations (0.2, 1, 2, 5, 10, 15 and 20 μM) of probe **F-2** was tested at 562 nm, and the mean value and standard deviation were obtained from three independent experimental measurements

increases rapidly with increasing reaction time, and the reaction of probe **F-2** with NaClO (65 eq) is nearly completed within 10 min. However, the result of the response time analysis obtained for probe **F-3** is different from that for probe **F-2**. The fluorescence intensity of probe **F-3** first decreased abruptly within 2 s after the addition of 150 eq NaClO, and then, it slowly increased and stabilized (Fig. S11). Although a slight enhancement in fluorescence was observed, the fluorescence intensity remained lower than that of the initial intensity. This result is consistent with the aforementioned titration results. Therefore, when NaClO was added, both probes **F-2** and **F-3** immediately showed a clear response with a short response time, indicating that probes **F-2** and **F-3** can be used for the rapid detection of ClO^-.

To assess the selectivity of probes **F-2** and **F-3** toward ClO^-, several substances and interfering ions (Ca^{2+}, H_2O_2, K^+, Br^-, HCO_3^-, HSO_3^-, I^-, NO_3^-, NH_4^+, and Zn^{2+}) were added to the detection system, respectively. As shown in Fig. S12, the absorbance and fluorescence intensity of probe **F-2** exhibits no distinct changes in comparison with those of the blank sample. Furthermore, the absorbance and fluorescence intensity of probe **F-3** did not significantly change with the addition of different interfering ions (Fig. S13). Therefore, probes **F-2** and **F-3** can selectively distinguish ClO^- from the other exogenous substances and ions.

Cytotoxicity and Fluorescent Imaging Analyses Using Fluorescent Probes F-2 and F-3

Considering that probes **F-2** and **F-3** will be used in future biological applications, MTT colorimetry was used to determine their cytotoxicity. The absorbance values of formazan at 562 nm were determined via three independent experiments at different concentrations (0.2–20 μM) to obtain the average cell survival rate. From Fig. 5, when the concentration of probe **F-2** is 0.1 μM, the cell survival rate is 98%. Even when the probe concentration was 20 μM, the cell survival rate was 90%. For probe **F-3**, the highest cell survival rate was 93% at a concentration of 0.1 μM, and the cell survival rate was 85% at a concentration of 20 μM (Fig. S14). In general, the cell survival rate observed for probe **F-2** was higher than that for probe **F-3**, indicating that probe **F-2** exhibits lower biotoxicity to cells than probe **F-3**.

Next, the ability of probes **F-2** and **F-3** for detecting ClO^- in living cells was examined using fluorescence confocal microscopy. Upon incubation with probe **F-2**, MCF-7 cells generated weak fluorescence. Furthermore, the fluorescence intensity did not increase with an extension of the monitoring time to 10 min (Fig. 6). However, when the MCF-7 cells were further treated with fresh NaClO (750 μM) for an additional 15 min, their fluorescence intensity increased from 139 to 211. Moreover, the fluorescence intensity increased from 211 to 294 with prolonged monitoring time (Fig. 7). Additionally, the detection of ClO^- in living cells using probe **F-3** was investigated (Fig. S15). The fluorescence intensity remained unchanged before the addition of exogenous ClO^-. As depicted in Fig. S16, the fluorescence intensity decreases from 215 to 54 after incubation with NaClO (750 μM) for additional 15 min. The aforementioned results indicate that both probes could be successfully used for the quantitative detection of ClO^- in living cells.

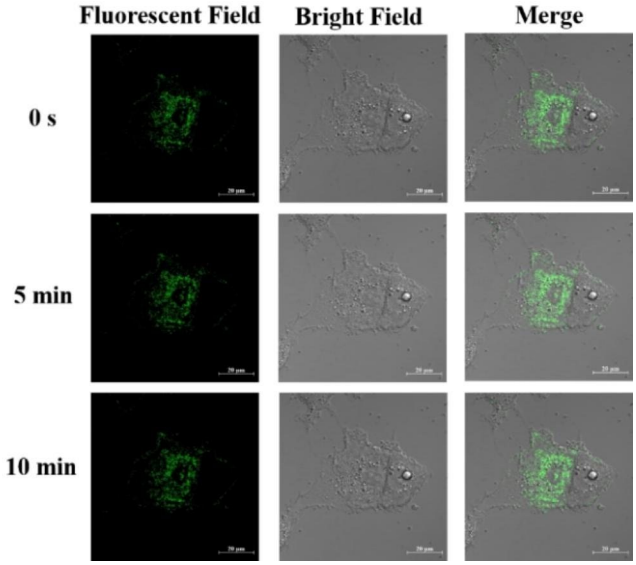

Fig. 6 Confocal fluorescence images of MCF-7 stained with probe **F-2** (15 μM) for 0.5 h without NaClO. Fluorescent images of the channels were collected at 520 ~ 580 nm; excitation wavelength was selected at 488 nm

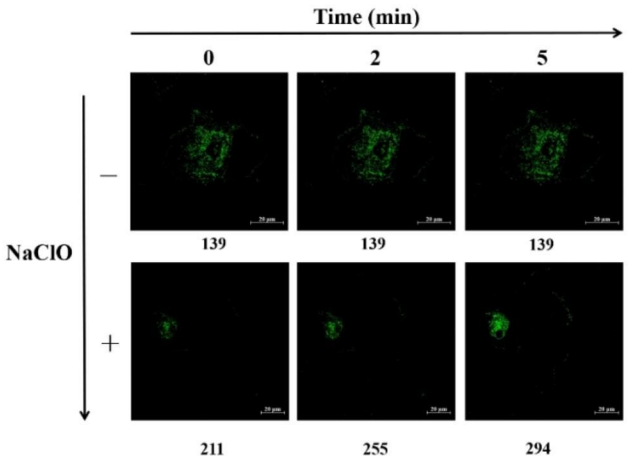

Fig. 7 Confocal fluorescence images of MCF-7 stained with **F-2** (15 μM) for 0.5 h before and after incubation with NaClO (750 μM). Fluorescent images of the channels collected at 520 ~ 580 nm; excitation wavelength at 488 nm. Notes: the number under the pictures stands for fluorescence intensity in vivo; the horizontal arrow stands for an extension of fluorescence monitoring time; the vertical arrow stands for the increase of NaClO concentration

Conclusions

In summary, two ClO^- fluorescent probes (**F-2** and **F-3**) were rationally designed and synthesized by introducing a C = N recognition functional group based on the fluorescein derivative **F-1**. LC–MS analysis confirmed the presence of by-product **F-3'** during the preparation of probe **F-3**. **F-3'** could be converted to **F-3** through a ring-opening reaction in a weakly alkaline system with a high yield. Gaussian calculation results reasonably revealed the electron cloud distribution of **F-2** and **F-3** in the ground and excited states and explained the photophysical properties of the synthesized probes. NaClO concentration titration and anti-interference analyses demonstrated that probes **F-2** and **F-3** could be used for the selective and fluorescent detection of ClO^- in solution based on the mechanism of imine deprotection by ClO^-. Cell toxicity analysis revealed that probes **F-2** and **F-3** possessed low biotoxicity and could be applied to detect ClO^- in vivo. Therefore, the synthesis and application of probes **F-2** and **F-3** are expected to be beneficial for the development of functional ClO^- probes in future.

Supplementary Information The online version contains supplementary material available at https://doi.org/10.1007/s10895-023-03495-7.

Authors' Contributions J. Zhu, Z. Lyu and X. Xiong contributed equally to this work. Junyang Zhu carried out the analytical measurements, data curation, and prepared original draft. Zhaoye Lyu synthesized the compounds and carried out the data curation. Yunan Qian carried out some data curation. Hailong Cui and Yutao Feng carried out the analytical measurements and some data curation. Miao Li was responsible for data management and review. Chengqi Jiao was responsible for supervision and validation, revision and funding acquisition. Xiaoqing Xiong was responsible for conceptualization, supervision and validation, methodology, writing-reviewing and editing, project administration and funding acquisition.

Funding This work was supported by the National Natural Science Foundation of China (21606032, 21903011, and 22108024), Youth Project of Liaoning Provincial Department of Education (LJKQZ2021117), Program of Natural Science Foundation of Liaoning Province (2022-MS-349), Dalian Youth Science and Technology Star Fund (2021RQ112), Dalian High-level Talent Innovation Support Program of China (2022RQ016).

Data Availability Data and materials will be made available on request.

Declarations

Ethical Approval Not applicable.

Competing interests The authors declare no competing interests.

References

1. Kim PA, Choe D, So H, Park S, Suh B, Jeong S, Kim KT, Kim C, Harrison RG (2021) A selective fluorescence sensor for hypochlorite used for the detection of hypochlorite in zebrafish. Spectrochim Acta A Mol Biomol Spectrosc 2021; 261: 120059
2. Shen SL, Zhang XF, Ge YQ, Zhu Y, Cao XQ (2018) A novel ratiometric fluorescent probe for the detection of HOCl based on FRET strategy. Sens Actuators B Chem 254:736–741
3. Yao SK, Qian Y (2017) A naphthalimide–rhodamine two-photon fluorescent turn-on probe for hypochlorous acid by desulfurization-cyclization and fluorescence resonance energy transfer. Sens Actuators B Chem 2017; 252: 877–885

4. Abdal Dayem A, Hossain MK, Lee SB, Kim K, Saha SK, Yang GM, Choi HY, Cho SG (2017) The role of reactive oxygen species (ROS) in the biological activities of metallic nanoparticles. Int J Mol Sci 18:120
5. He X, Deng Z, Xu W, Li Y, Xu C, Chen H, Shen J (2020) A novel dual-response chemosensor for bioimaging of Exogenous/Endogenous hypochlorite and hydrazine in living cells, Pseudomonas aeruginosa and zebrafish. Sens Actuators B Chem 321:128450
6. Shen BX, Qian Y, Qi ZQ, Lu CG, Sun Q, Xia X, Cui YP (2017) Near-infrared BODIPY-based two-photon ClO^- probe based on thiosemicarbazide desulfurization reaction: naked-eye detection and mitochondrial imaging. J Mater Chem B 5:5854–5861
7. Nguyen VN, Heo S, Kim S, Swamy K, Ha J, Park S, Yoon J (2020) A thiocoumarin-based turn-on fluorescent probe for hypochlorite detection and its application to live-cell imaging. Sens Actuators B Chem 317:128213
8. Yap YM, Whiteman M, Cheung NS (2007) Chlorinative stress: an under appreciated mediator of neurodegeneration? Cell Signal 19:219–228
9. Mainnemare A, Mégarbane B, Soueidan A, Daniel A, Chapple ILC (2004) Hypochlorous acid and taurine-N-monochloramine in periodontal Diseases. J Dent Res 83:823–831
10. Huang KC, Yang CC, Lee KT, Chien CT (2003) Reduced hemodialysis-induced oxidative stress in end-stage renal Disease patients by electrolyzed reduced water. Kidney Int 64:704–714
11. Wang L, Pan Q, Chen Y, Ou Y, Li H, Li B (2020) A dual-response ratiometric fluorescent probe for hypochlorite and hydrazine detection and its imaging in living cells. Spectrochim Acta A Mol Biomol Spectrosc 241:118672
12. Chen X, Wang F, Hyun JY, Wei T, Qiang J, Ren X, Shin I, Yoon J (2016) Recent progress in the development of fluorescent, luminescent and colorimetric probes for detection of reactive oxygen and nitrogen species. Chem Soc Rev 45:2976–3016
13. Tang Y, Lee D, Wang J, Li G, Yu J, Lin W, Yoon J (2015) Development of fluorescent probes based on protection–deprotection of the key functional groups for biological imaging. Chem Soc Rev 44:5003–5015
14. Goswami S, Das AK, Manna A, Maity AK, Saha P, Quah CK, Fun HK, Abdel-Aziz HA (2014) Nanomolar detection of hypochlorite by a rhodamine-based chiral hydrazide in absolute aqueous media: application in tap water analysis with live-cell imaging. Anal Chem 86:6315–6322
15. Bao X, Cao X, Yuan Y, Zhou B, Huo C (2021) A water-soluble, highly sensitive and ultrafast fluorescence probe for imaging of mitochondrial hypochlorous acid. Sens Actuators B Chem 344:130210
16. Chen M, Chen X, Wang Y, Fan X, Chen T, Liang Z (2022) An ESIPT fluorescent probe for ultrarapid HClO detection during reagent-stimulated oxidative stress in cells and zebrafish. Sens Actuators B Chem 371:132545
17. Li P, Jia Y, Zhao N, Zhang Y, Zhou P, Lou Z, Qiao Y, Zhang P, Wen S, Han K (2020) Quantifying the fast dynamics of HClO in living cells by a fluorescence probe capable of responding to oxidation and reduction events within the time scale of milliseconds. Anal Chem 92:12987–12995
18. Shao S, Yang T, Han Y (2023) A TICT-based fluorescent probe for hypochlorous acid and its application to cellular and zebrafish imaging. Sens Actuators B Chem 392:134041
19. Teng H, Tian J, Sun D, Xiu M, Zhang Y, Qiang X, Tang H, Guo Y (2020) A mitochondria-specific fluorescent probe based on triazolopyridine formation for visualizing endogenous hypochlorous acid in living cells and zebrafish. Sens Actuators B Chem 319:128288
20. Chen X, Jiang D, Jiang C, Yao C (2023) A novel near-infrared ratiometric fluorescent probe targeting lysosomes for imaging HOCl in vitro and in vivo. Spectrochim Acta A Mol Biomol Spectrosc 286:121966
21. Bi S, Yang T, An K, Zhou B, Han Y (2023) A benzo BODIPY based fluorescent probe for selective visualization of hypochlorous acid in living cells and zebrafish. Spectrochim Acta A Mol Biomol Spectrosc 299:122860
22. Wei H, Tan M, Lin Y, Chen H, Wu X, Zhang Z, Ke F (2023) A highly selective fluorescent probe for the detection of exogenous and endogenous hypochlorous acid/hypochlorite. Chem Pap 77:2317–2325
23. Wang D, Chen, Kambam S, Wang F, Wang Y, Zhang W, Yin J, Chen H, Chen X (2015) A highly specific fluorescent probe for hypochlorite based on fluorescein derivative and its endogenous imaging in living cells. Dyes Pigm 120:22–29
24. Gil D, Lee JJ, Lee H, Kim KT, Kim C (2022) Detection of environmentally hazardous hypochlorite in pure water with a novel fluorescent chemosensor: application to water samples, commercial disinfectants, test strips, and zebrafish. Dyes Pigm 207:110714
25. Teng H, Tian J, Sun D, Xiu M, Zhang Y, Qiang X, Tang H, Guo Y (2020) A mitochondria-specific fluorescent probe based on triazolopyridine formation for visualizing endogenous hypochlorous acid in living cells and zebrafish. Sens Actuators B Chem 319:128288
26. Wu WL, Zhao ZM, Dai X, Su L, Zhao BX (2016) A fast-response colorimetric and fluorescent probe for hypochlorite and its real applications in biological imaging. Sens Actuators B Chem 232:390–395
26. Ning Y, Cui J, Lu Y, Wang X, Xiao C, Wu S, Li J, Zhang Y (2018) De novo design and synthesis of a novel colorimetric fluorescent probe based on naphthalenone scaffold for selective detection of hypochlorite and its application in living cells. Sens Actuators B Chem 269:322–330
28. Li J, Yang X, Zhang D, Liu Y, Tang J, Li Y, Zhao Y, Ye Y (2018) A fluorescein-based turn-on fluorescence probe for hypochlorous acid detection and its application in cell imaging. Sens Actuators B Chem 265:84–90
29. Yan F, Fan K, Ma T, Xu J, Wang J, Ma C (2019) Synthesis and spectral analysis of fluorescent probes for Ce^{4+} and OCl^- ions based on fluorescein Schiff base with amino or hydrazine structure: application in actual water samples and biological imaging. Spectrochim Acta A Mol Biomol Spectrosc 213:254–262
30. Xiong X, Song F, Chen G, Sun W, Wang J, Gao P, Zhang Y, Qiao B, Li W, Sun S, Fan J, Peng X (2013) Construction of long-wavelength fluorescein analogues and their application as fluorescent probes. Chem Eur J 19:6538–6545
31. Xiong X, Yuan Y, Chen G, Li M, Lyu L, Zhao H, Yan J, Qian Y, Zhu J, Jiao C (2023) Construction, photophysical properties, structure-activity relationship, and applications of fluorescein analogs. Dyes Pigm 208:110870